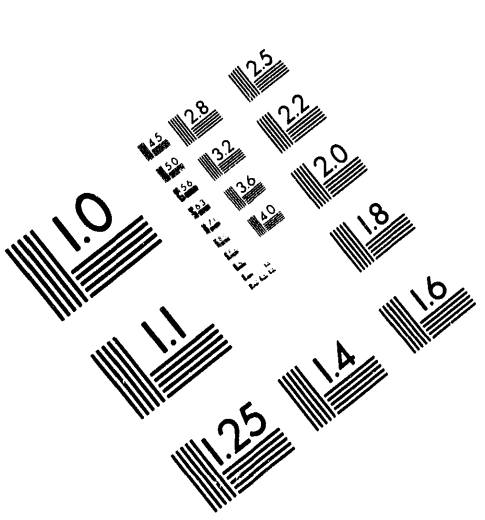

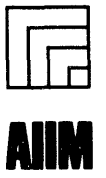

AIIM

Association for Information and Image Management
1100 Wayne Avenue, Suite 1100
Silver Spring, Maryland 20910
301/587-8202

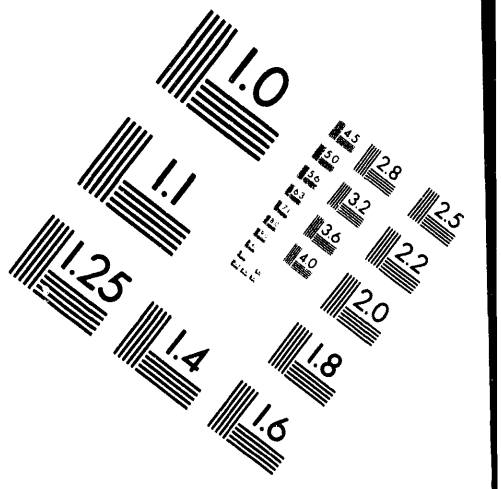

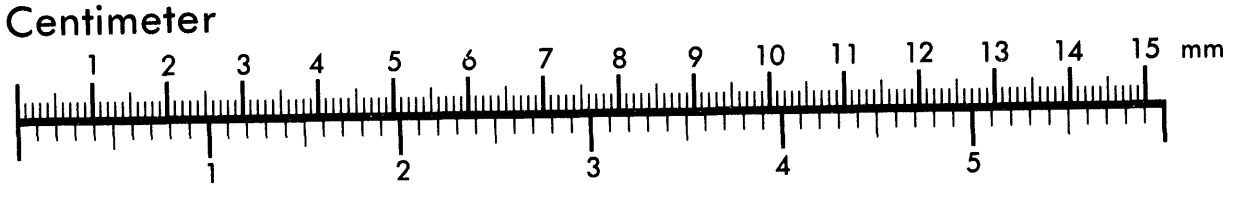

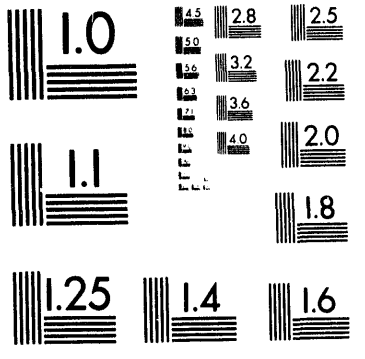

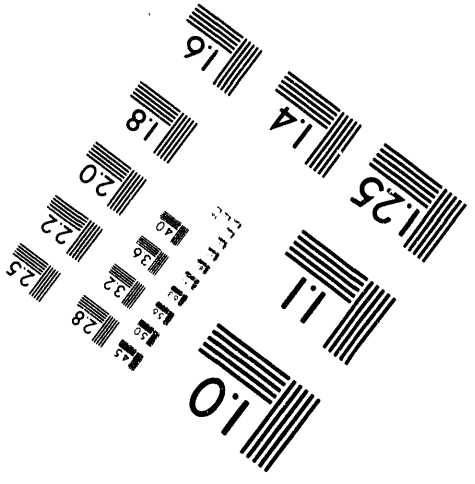

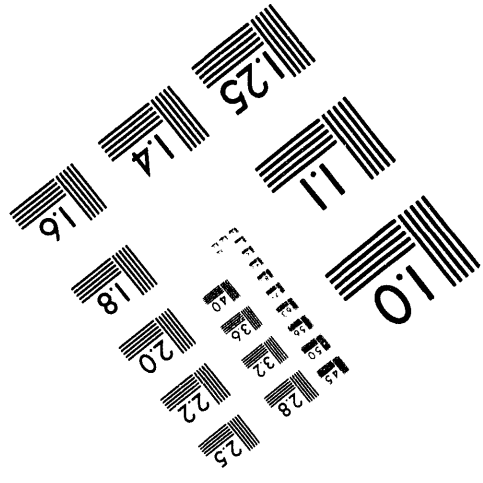

MANUFACTURED TO AIIM STANDARDS
BY APPLIED IMAGE, INC.

1 of 1

Conf-941142--7

LA-UR-94-1470

Los Alamos National Laboratory is operated by the University of California for the United States Department of Energy under contract W-7405-ENG-36

TITLE: A LAGRANGIAN PARTICLE METHOD FOR THE SIMULATION OF DENSE PARTICULATE FLOWS

AUTHOR(S): M(alcolm) J. Andrews, Texas A&M
D. A. J. Baillergeau, Ecole Polytechnique
P(eter) J. O'Rourke, T-3

SUBMITTED TO: *ASME Winter Meeting, Chicago, Illinois, November 6–9, 1994*

Los Alamos

Los Alamos National Laboratory
Los Alamos, New Mexico 87545

FORM NO. 836 R4
ST. NO. 2629 5/81

A LAGRANGIAN PARTICLE METHOD FOR THE SIMULATION OF DENSE PARTICULATE FLOWS

M. J. Andrews
Department of Mechanical Engineering
Texas A&M University
College Station, TX 77843-3123

D.A.J. Baillergeau
Ecole Polytechnique
Paris, France

P.J. O'Rourke
Los Alamos National Laboratory
Los Alamos, NM 87545

ABSTRACT

A new approach to the simulation of multi-phase dense particulate flows has been developed based on taking the best of Eulerian/Eulerian and Eulerian/Lagrangian formulations. This new approach uses a modern Particle-In-Cell method that has been extended to multi-phase flows. The method uses accurate mappings from Lagrangian particles to and from Eulerian space so that continuum intergranular stress formulations can be incorporated in the modeling. The result is a new model that can handle particulate loading ranging from dense to dilute, a distribution of particle sizes, and a range of particulate materials. This paper describes the new method and results from a one-dimensional implementation. The Lagrangian particulate formulation is well suited for a massively parallel environment, with a coupled high speed calculation of the underlying Eulerian gas phase governing equations. The new simulation method has important applications in Fluidized Bed Combustion, Catalytic Cracking processes and many other granular flows. Extension of the method to two- and three-dimensional flows with parallel computation means that we can offer a comprehensive methodology for dense granular flows.

NOMENCLATURE

A	Particle acceleration, equation (4)
D	Drag function, equation (16)
I	Interaction between particles, equation (15)
P	Mean gas pressure
$S(x)$	Linear interpolation function, equation (24)
T	Slope function, equation (31)
f	Solid phase distribution function
g	Gravitational acceleration
u_g	Gas velocity
u_s	Mass average solid velocity
v_p	Solid particle velocity
Δt	Numerical time step
Δx	Numerical cell size
ε	Gas void fraction
θ	Solid void fraction
θ_0	Initial solid void fraction
ρ_g	Gas density (mass of gas per unit gas volume)
ρ_s	Solid (particle) density
τ	Solid stress

Superscripts

n	Evaluated at time $n\Delta t$.

Subscripts

p	Particle.
s	Solids.
g	Gas.
i	Cell center index.
$i+1/2$	Cell index of right face.

INTRODUCTION

Modeling of two-phase particulate flows may be divided into Locally Homogenous Flow (LHF) models, and Separated Flow (SF) models. In homogeneous flow systems the two components of the system move with the same local velocity so mixture equations can be readily formulated. In separated flow systems the two components have separate, but not necessarily the same, velocities that exert an influence on one another through such terms as drag and mean gas pressure gradient. This separated flow formulation is the more general form and the one of interest in this work. Kuo (1986) gives a more complete discussion of two-phase flow models.

Mathematical models of separated particulate two phase flow have been either a Lagrangian description for the particulate phase and a Eulerian continuum description for the gas phase, or a Eulerian continuum description for both phases. The Lagrangian/Eulerian description is well suited for disperse particulate flows with particulate void fractions of up to about 5%, typical applications are sprays, Andrews and Bracco (1991), and Andrews (1993). When the particulate void fractions are above 5%, the particle collision frequency is high and cannot not be realistically resolved with a Lagrangian collision calculation.

The continuum Eulerian/Eulerian formulation is most appropriate for particulate void fractions above 5%. Under these circumstances the particulate phase is treated as a fluid with mixture properties and collisions handled by intergranular stress terms expressed through continuum spatial gradients, Gidaspow (1986). Such a formulation works well when the particulate size distribution is monotonic. However, when a particle size distribution is modeled, equations must be introduced to follow the movement of the different particle sizes in the flow. Thus, many equations may need to be applied that require additional storage and an unnecessary calculation for particle distribution concentrations where there may be no particles of that size, Rizk (1993).

Here we present a numerical simulation procedure for multi-phase flows that consistently blends Lagrangian/Eulerian and Eulerian/Eulerian methods. The computation of Lagrangian particle coefficients is well suited to a massively parallel environment. We start by presenting the governing equations of two phase flow and then a one-dimensional implementation of the simulation procedure. Three validation calculations then follow that demonstrate the methodology. The paper closes with conclusions and references.

FORMULATION

Our interest is in fluidized beds with a two-phase flow comprising solid particles moving in a gas phase. The gas phase is considered to be a continuum. The major problem is to describe the interaction between the solid particles and the gas. In the following section governing equations are developed based on an approach that can handle flows with a wide range of particle sizes. However, this approach introduces difficulties with particle-particle interactions, so we introduce averaging procedures to obtain a particulate phase continuum formulation for which we have taken the empirical relations of Gidsapow (1986).

Governing equations of the gas phase

The gas is perfect and with constant entropy, so p/ρ_g^{γ} = constant and inviscid (gas viscosity is reintroduced when gas-particle drag is considered). The gas continuity equation is:

$$\frac{\partial(\varepsilon\rho_g)}{\partial t}+\nabla_x\cdot(\varepsilon\rho_g\underline{u}_g)=0 \qquad (1)$$

where ε is the gas void fraction, ρ_g is the gas density (based on mass of gas per unit gas volume), and $\underline{u}_g$ is the gas velocity. The gas momentum equation is:

$$\frac{\partial(\varepsilon\rho_g\underline{u}_g)}{\partial t}+\nabla_x\cdot(\varepsilon\rho_g\underline{u}_g\underline{u}_g)=-\varepsilon\nabla_x P-\underline{F}-\rho_g\varepsilon\underline{g} \qquad (2)$$

where P is the gas pressure, $\underline{g}$ gravity, and F the momentum exchange between gas and particulate phases.

Governing equations of the solid phase

Evolution of the solid phase distribution function $f(\underline{x}, \underline{v}, m, t)$ is governed by:

$$\frac{\partial f}{\partial t}+\nabla_x\cdot(\underline{v}f)+\nabla_v\cdot(\underline{A}f)=0 \qquad (3)$$

where $\underline{A}$ is the particle acceleration, $\underline{x}$ is the position of the particle, $\underline{v}$ is the particle velocity, m is particle mass, and t is time. In the present work we have assumed the solid phase density and particle density are the same, but this is not an intrinsic limitation of the method. The expression for A is:

$$\underline{A}=D\left(m,\left|\underline{u}_g-\underline{v}_p\right|\right)\left(\underline{u}_g-\underline{v}_p\right)-\frac{1}{\rho_s}\nabla_x P-\underline{g}+\underline{L} \qquad (4)$$

where D is a drag function described later and depends on the local particle Reynolds number. The second term in equation (4) accounts for the mean gas pressure gradient, the third term is gravity, and the last term, $\underline{L}$ represents the interaction between particles.

It is useful to show that Lagrangian and Eulerian descriptions of the solid phase are equivalent except for terms that are intrinsic to each formulation. To obtain average variables for an Eulerian formulation that will depend only on $\underline{x}$ and t, we integrate equation (3) over $\underline{v}$ and m, having multiplied by m or $m\underline{v}$ to give the mass or momentum equations. For the mass:

$$\int_{v,m}\left\{m\frac{\partial f}{\partial t}+m\nabla_x\cdot(\underline{v}f)+m\nabla_v\cdot(\underline{A}f)\right\}d\underline{v}dm=0 \qquad (5)$$

The mass m of each particle is constant so equation (5) may be rewritten as:

$$\frac{\partial}{\partial t}\left(\int_{v,m}mf\,d\underline{v}dm\right)+\nabla_x\cdot\left(\int_{v,m}m\underline{v}f\,d\underline{v}dm\right)=0 \qquad (6)$$

Defining $\theta\rho_s=\int_{v,m}mfd\underline{v}dm$, θ is the mass fraction of the solid phase and satisfies $\theta+\varepsilon=1$, ρ_s the solid phase density, and $\theta\rho_s\underline{u}_s=\int_{v,m}m\underline{v}fd\underline{v}dm$, where $\underline{u}_s$ is the mass average solid velocity. Equation (6) may be written in the more familiar form:

$$\frac{\partial(\theta\rho_s)}{\partial t}+\nabla_x\cdot\left(\theta\rho_s\underline{u}_s\right)=0 \qquad (7)$$

The momentum equation is:

$$\int_{v,m}\left\{m\underline{v}\frac{\partial f}{\partial t}+m\underline{v}\nabla_x\cdot(\underline{v}f)+m\underline{v}\nabla_v\cdot(\underline{A}f)\right\}d\underline{v}dm=0 \qquad (8)$$

or for each velocity component i:

$$\int_{v,m}\left\{mv_i\frac{\partial f}{\partial t}+mv_i\frac{\partial}{\partial x_j}(v_jf)+mv_i\frac{\partial}{\partial v_j}(A_jf)\right\}d\underline{v}dm=0 \qquad (9)$$

Since $\underline{v}$ is the space of velocities we may write the first term as:

$$\int_{v,m}mv_i\frac{\partial f}{\partial t}d\underline{v}dm=\frac{\partial(\theta\rho_s u_{si})}{\partial t} \qquad (10)$$

with u_{si} the i^{th} component of $\underline{u}_s$. The second term in equation (9) may be written as:

$$\int_{v,m}mv_i\frac{\partial}{\partial x_j}(v_jf)d\underline{v}dm=\frac{\partial}{\partial x_j}(u_{si}u_{sj}\theta\rho_s)+\frac{\partial}{\partial x_j}\int_{v,m}mf(v_i')(v_j')d\underline{v}dm \qquad (11)$$

where $v_i'=v_i-u_{si}$, and $v_j'=v_j-u_{sj}$ are local particle velocity fluctuations around the average velocity. The third term in equation (9) may be written as:

$$\int_{v,m}mv_i\frac{\partial}{\partial v_j}(fA_j)\,d\underline{v}dm=\int_{v,m}\frac{\partial}{\partial v_j}(mv_ifA_j)\,d\underline{v}dm-\int_{v,m}(mfA_i)\,d\underline{v}dm \qquad (12)$$

Using Gauss's theorem, the first term of the right-hand side is zero because $f = 0$ for small and large v. The final solid phase momentum equation is:

$$\frac{\partial}{\partial t}(\theta\rho_s u_{si}) + \nabla_x \cdot (\theta\rho_s u_{si}\underline{u}_s) = -\nabla_x \cdot \int mf(v_{pi} - u_{si})(\underline{v}_p - \underline{u}_s)\, d\underline{v}dm + \int_{v,m} mfA_i\, d\underline{v}dm \quad (13)$$

Inserting the expression (4) for A we obtain for the mean gas pressure gradient and gravitational terms:

$$-\int_{v,m} mf\nabla_x P\, d\underline{v}dm = -\theta\nabla_x P \text{ and } \int_{v,m} \underline{g}mf\, d\underline{v}dm = \theta\rho_s \underline{g} \quad (14)$$

For the interaction term we take the empirical formula proposed by Gidaspow of $\int_{v,m} mf\underline{I}\, d\underline{v}dm = \nabla_x \tau$, where τ is the solid stress. In our Lagrangian formulation, as a first approximation, we take I as independent of size and velocity giving:

$$\underline{I} = \frac{1}{\theta\rho_s}\nabla_x \tau \quad (15)$$

For the drag function we use the expression of O'Rourke (1981):

$$D = C_d \frac{3}{8}\frac{\rho_g |\underline{u}_g - \underline{v}_p|}{r} \quad (16)$$

with $C_d = \frac{24}{R_e}\left(\varepsilon^{-2.65} + \frac{R_e^{2/3}}{6}\varepsilon^{-1.78}\right)$, and $R_e = \frac{2\rho_g |\underline{u}_g - \underline{v}_p| r}{\mu_g}$. In the limit of small solid fractions this formulation reduces to the expressions proposed by Putnam (1961) for solid spheres. The ε dependence corresponds with that found in the experiments of Richardson (1954).

The first term on the right-hand side of equation (13) does not appear in many formulations of particle continuum equations. In the present formulation this additional term arises as a kinematic stress that considers local particle velocity fluctuations around the average velocity.

Summary of governing equations in one dimension

In one-dimension the resulting governing equations for the gas phase continuity and momentum are:

$$\frac{\partial(\varepsilon\rho_g)}{\partial t} + \frac{\partial(\varepsilon\rho_g u_g)}{\partial x} = 0$$

$$\frac{\partial(\varepsilon\rho_g u_g)}{\partial t} + \frac{\partial(\varepsilon\rho_g u_g^2)}{\partial x} = -\varepsilon\frac{\partial P}{\partial x} - \int_{v,m} fmD\left(m, |u_g - v_p|\right)(u_g - v_p)\, dvdm - \rho_g \varepsilon g \quad (17)$$

The solid phase Eulerian governing equations are:

$$\frac{\partial(\theta\rho_s)}{\partial t} + \frac{\partial(\theta\rho_s u_s)}{\partial x} = 0$$

$$\frac{\partial(\theta\rho_s u_s)}{\partial t} + \frac{\partial(\theta\rho_s u_s^2)}{\partial x} = -\theta\frac{\partial P}{\partial x} + \int_{v,m} fmD\left(m, |u_g - v_p|\right)(u_g - v_p)\, dvdm - \nabla_x \cdot \int mf(v_{pi} - u_{si})(\underline{v}_p - \underline{u}_s)\, d\underline{v}dm - \theta\rho_s g - \frac{\partial\tau}{\partial x} \quad (18)$$

Following Gidaspow (1986) we take $\frac{\partial\tau}{\partial x} = G(\varepsilon)\frac{\partial\varepsilon}{\partial x}$, where the modulus of elasticity is given by:

$$G(\varepsilon) = \frac{\partial\tau}{\partial\varepsilon} = 10^{\alpha(1-\varepsilon)+\beta} \text{ with } \alpha = -8.76 \text{ and } \beta = 5.43 \quad (19)$$

The equations that describe individual particle motion are:

$$\frac{\partial x_p}{\partial t} = v_p$$

$$\frac{\partial v_p}{\partial t} = D_p\left(m, |u_g - v_p|\right)(u_g - v_p) - g - \frac{1}{\rho_s}\frac{\partial P}{\partial x} - \frac{1}{\rho_s\theta}\frac{\partial\tau}{\partial x} \quad (20)$$

The continuum, equation (18) , and Lagrangian-particle, equation (19), formulations for the solid phase illustrate the two approaches to modeling two-phase flows. Empirical expressions for the solids stresses are easy to incorporate in the continuum formulation, but to eliminate the distribution function, f, which we do not solve, the kinematic stress term of equation (18) is ignored and the drag term is simplified by assuming particles of a single size and velocity. However, the Lagrangian formulation accounts for the effects of a distribution of sizes and velocities but further assumptions must be made to relate solids stress to the collisional force on an individual particle. When detailed theories have been developed that give the average collisional force on a particle as a function of velocity and size, this information can be incorporated into the Lagrangian formulation, thereby providing a more detailed and fundamental approach to computing solids stress.

Next we solve the equations of the Lagrangian-particle formulation. The gas-phase equations (17) are solved on a Eulerian grid. We do not directly solve the coupled equations of the particle and gas phases because this would involve a computationally costly iterative, implicit solution for the velocity of each particle. Instead, we interpolate the particle properties to the grid and solve implicit approximations to the particle continuum equations and gas phase equations on the grid. Terms needed to update particle properties, such as the local gas velocity and pressure gradient, are interpolated back to each particle and used in a final explicit calculation of particle velocities and positions.

NUMERICAL SOLUTION OF THE GOVERNING EQUATIONS

Next we develop a finite difference method for the gas phase, and then the solid particle phase is described with computational particles that each represent several real particles. We use a PIC method, Harlow (1964), however particle quantities are accurately interpolated onto the numerical grid to introduce average quantities for use in evaluating the solids stress. We then solve the governing equations using these quantities and map back to the individual particle quantities. These forward and backward interpolations between discrete and continuous representations of particle exchange terms allows flexibility to choose the most appropriate mathematical formulation. We retain numerical accuracy by using second order accurate interpolations.

Figure 1 shows the computational. A staggered formulation of velocities and scalars is used, with cell index i defined at the cell center, and $i+\frac{1}{2}$ at the right-hand cell face. The superscript 'n' refers to the value at the n^{th} time step, $n\Delta t$.

Numerical formulation for the particle governing equations

Each particle p represents N_p real particles with mass m_p, velocity v_p, and position x_p. The equations (20) are numerically represented as:

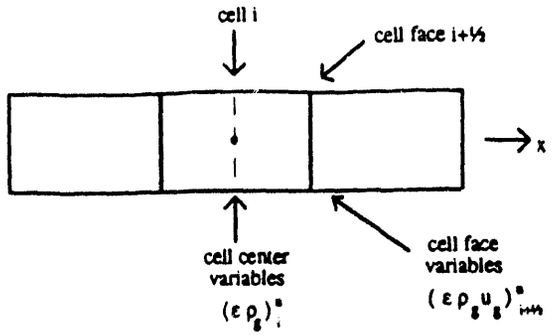

Figure 1. Numerical grid and definitions.

$$x_p^{n+1} = x_p^n + v_p^{n+1}\Delta t \tag{21}$$

$$\frac{v_p^{n+1} - v_p^n}{\Delta t} = D_p^n\left(u_g^{n+1} - v_p^{n+1}\right) - g - \frac{1}{\rho_s}\left(\frac{\partial P}{\partial x}\right)_p^{n+1} - \frac{1}{\rho_s\tilde{\theta}_p}\left(\frac{\partial \tau}{\partial x}\right)_p^{n+1} \tag{22}$$

where D_p^n is the drag function evaluated at time t_n and $\tilde{\theta}_p$ is an approximation of the solid void fraction described below.

To evaluate solid phase continuum interaction terms, such as the last term of equation (22), we next develop a solid phase continuity equation. The solid phase void fraction in cell i is defined as:

$$\theta_i^n = \frac{1}{\Delta x}\sum_p S_i\left(x_p^n\right)\frac{m_p}{\rho_s}N_p \tag{23}$$

where for non boundary cells S_i is a linear interpolation function, shown in figure 2, for $i \neq 1$ or $i \neq N_{cell}$ (N_{cell} is the number of cells) then:

$$S_i(x) = \begin{cases} \dfrac{x - x_{i-1}}{\Delta x} & \text{if} \quad x_{i-1} \le x \le x_i \\ \dfrac{x_{i+1} - x}{\Delta x} & \text{if} \quad x_i \le x \le x_{i+1} \\ 0 & \text{if} \quad x < x_{i-1} \quad \text{or} \quad x > x_{i+1} \end{cases} \tag{24}$$

where x_i is the x position of the center of the cell i.

For the lower boundary cell at $i = 1$, as shown in figure 3, we use:

$$S_1(x) = \begin{cases} 1 & \text{if} \quad 0 \le x \le x_1 \\ \dfrac{x_2 - x}{\Delta x} & \text{if} \quad x_1 \le x \le x_2 \\ 0 & \text{if} \quad x > x_2 \end{cases} \tag{25}$$

For the last cell boundary at $i = N_{cell}$

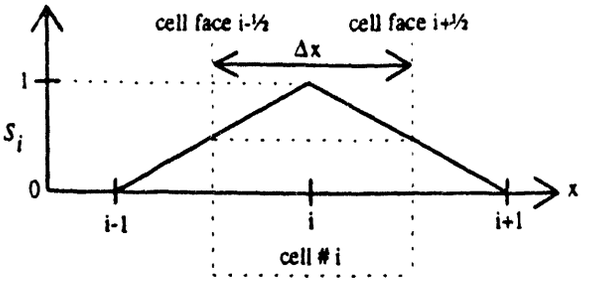

Figure 2. Linear interpolation function for domain cells.

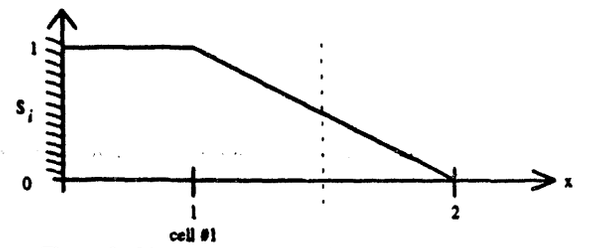

Figure 3. Linear interpolation function at the first cell.

$$S_{N_{cell}}(x) = \begin{cases} \dfrac{x - x_{N_{cell}-1}}{\Delta x} & \text{if} \quad x_{N_{cell}-1} \le x \le x_{N_{cell}} \\ 1 & \text{if} \quad x_{N_{cell}} \le x \le x_{last} \\ 0 & \text{if} \quad x < x_{N_{cell}-1} \end{cases} \tag{26}$$

where x_{last} is the x position of the end of the domain. The choice for S_1 and $S_{N_{cell}}$ is made to ensure $\sum_i S_i(x) = 1$ for all values of x.

The change of θ_i over a time step is given by:

$$\theta_i^{n+1} - \theta_i^n = \frac{1}{\Delta x}\sum_p\left[S_i\left(x_p^{n+1}\right) - S_i\left(x_p^n\right)\right]\frac{m_p}{\rho_s}N_p \tag{27}$$

The following equation determines an intermediate position of a particle:

$$\tilde{x}_p^n = x_p^n + v_p^n\Delta t \tag{28}$$

The interpolation function at x_p^{n+1} is given by:

$$S_i\left(x_p^{n+1}\right) \approx S_i\left(\tilde{x}_p^n\right) + \left(x_p^{n+1} - \tilde{x}_p^n\right)\frac{\partial S_i}{\partial x}\left(\tilde{x}_p^n\right) \tag{29}$$

Combining equations (21) and (28) gives:

$$x_p^{n+1} - \tilde{x}_p^n = \left(v_p^{n+1} - v_p^n\right)\Delta t \tag{30}$$

We define a slope function such that:

$$T_{i+\frac{1}{2}}(x) = \begin{cases} 1 & \text{if} \quad x_i \le x \le x_{i+1} \\ 0 & \text{if} \quad x < x_i \quad \text{or} \quad x > x_{i+1} \end{cases} \tag{31}$$

Then $\dfrac{\partial S_i(x)}{\partial x}$ may be conveniently written as:

$$\frac{\partial S_i(x)}{\partial x} = \frac{1}{\Delta x}\left(T_{i-\frac{1}{2}} - T_{i+\frac{1}{2}}\right) \tag{32}$$

Using equations (29), (30) and (32), equation (27) is written as:

$$\frac{\theta_i^{n+1}-\theta_i^n}{\Delta t}+\left.\frac{\partial(\theta u_i)}{\partial x}\right|_{explicit}+\frac{(\theta\delta u_i)_{i+\frac{1}{2}}-(\theta\delta u_i)_{i-\frac{1}{2}}}{\Delta x}=0 \qquad (33)$$

with the following definitions:

$$\left.\frac{\partial(\theta u_i)}{\partial x}\right|_{explicit}\equiv\frac{1}{\Delta x}\sum_p\left[\frac{S_i(x_p^n)-S_i(\tilde{x}_p^n)}{\Delta t}\right]\frac{m_pN_p}{\rho_s} \qquad (34)$$

$$(\theta\delta u_s)_{i+\frac{1}{2}}\equiv\frac{1}{\Delta x}\sum_p\frac{m_pN_p}{\rho_s}T_{i+\frac{1}{2}}(\tilde{x}_p^n)(v_p^{n+1}-v_p^n) \qquad (35)$$

The new particle velocity is calculated with equation (26) as:

$$v_p^{n+1}=\frac{v_p^n+\Delta t\left[D_p^n u_{g,p}^{n+1}-g-\frac{1}{\rho_s}\left(\frac{\partial P_s}{\partial x}\right)_p^{n+1}-\frac{1}{\rho_s\tilde{\theta}_p^n}\left(\frac{\partial\tau}{\partial x}\right)_p^{n+1}\right]}{1+\Delta tD_p^n} \qquad (36)$$

with:

$$\tilde{\theta}_p^n=\sum_i T_{i+\frac{1}{2}}(\tilde{x}_p)\tilde{\theta}_{i+\frac{1}{2}}^n \text{ and } \tilde{\theta}_{i+\frac{1}{2}}^n=\frac{1}{\Delta x}\sum_p\frac{N_pm_p}{\rho_s}T_{i+\frac{1}{2}}(\tilde{x}_p) \qquad (37)$$

Where $u_{g,p}^{n+1}$ is an interpolated gas velocity given later. The terms $\left(\frac{\partial P}{\partial x}\right)_p^{n+1}$ and $\left(\frac{\partial\tau}{\partial x}\right)_p^{n+1}$ are implicit expressions using the value of pressure P and τ at time $n+1$ in the particle cell, and are evaluated as:

$$\left(\frac{\partial P}{\partial x}\right)_p^{n+1}=\frac{P_{i_p+1}^{n+1}-P_{i_p}^{n+1}}{\Delta x} \text{ and } \left(\frac{\partial\tau}{\partial x}\right)_p^{n+1}=\frac{\tau_{i_p+1}^{n+1}-\tau_{i_p}^{n+1}}{\Delta x} \qquad (38)$$

where i_p denotes the cell index such that $x_{i_p}<x_p<x_{i_p+1}$.
Substituting expression (36) into (35) gives:

$$(\theta\delta u_s)_{i+\frac{1}{2}}=\frac{1}{\Delta x}\sum_p\frac{m_pN_p}{\rho_s}T_{i+\frac{1}{2}}(\tilde{x}_p^n)\frac{\Delta t\left[D_p^n\left(u_{g,p}^{n+1}-v_p^n\right)-g-\frac{1}{\rho_s}\left(\frac{\partial P}{\partial x}\right)_p^{n+1}-\frac{1}{\rho_s\tilde{\theta}_p^n}\left(\frac{\partial\tau}{\partial x}\right)_p^{n+1}\right]}{1+\Delta tD_p^n} \qquad (39)$$

Equation (33) is the solid mass void fraction update equation, with mass fluxes computed with equations (34) and (39). Similarly the particle velocities are updated with equation (36). However, gas phase terms implicitly appear in these equations and their evaluation is described next.

Gas governing equations

Two variables, $(\varepsilon\rho_g)_i^n$ and $(\varepsilon\rho_g u_g)_{i+\frac{1}{2}}^n$ describe the gas, and the gas continuity equation becomes:

$$\frac{(\varepsilon\rho_g)_i^{n+1}-(\varepsilon\rho_g)_i^n}{\Delta t}+\frac{(\varepsilon\rho_g u_g)_{i+\frac{1}{2}}^{n+1}-(\varepsilon\rho_g u_g)_{i-\frac{1}{2}}^{n+1}}{\Delta x}=0 \qquad (40)$$

where $(\varepsilon\rho_g)_i^n$ is a cell center variable and $(\varepsilon\rho_g u_g)_{i+\frac{1}{2}}^n$ is the mass flux through the right side cell face, as shown in figure 1. The gas momentum equation is written as:

$$\frac{(\varepsilon\rho_g u_g)_{i+\frac{1}{2}}^{n+1}-(\varepsilon\rho_g u_g)_{i+\frac{1}{2}}^n}{\Delta t}+\frac{(\varepsilon\rho_g u_g^2)_{i+1}^n-(\varepsilon\rho_g u_g^2)_i^n}{\Delta x}+\frac{P_{i+1}^{n+1}-P_i^{n+1}}{\Delta x}=E_x-(\varepsilon\rho_g)_{i+\frac{1}{2}}^{n+1}g \qquad (41)$$

The exchange term, E_x, includes the source of momentum from each particle given by:

$$E_x=\sum_p T_{i+\frac{1}{2}}(\tilde{x}_p^n)\left[-D_p^n\left(u_{g,p}^{n+1}-v_p^{n+1}\right)+\frac{1}{\rho_s}\left(\frac{\partial P}{\partial x}\right)_p^{n+1}\right]N_p \qquad (42)$$

This expression can be re-written with the following definitions:

$$u_{g,p}^{n+1}=\sum_i T_{i+\frac{1}{2}}(\tilde{x}_p)\frac{(\rho_g\varepsilon u_g)_{i+\frac{1}{2}}^{n+1}}{(\rho_g\varepsilon)_{i+\frac{1}{2}}^n} \quad \text{and}$$

$$(\rho_g\varepsilon)_{i+\frac{1}{2}}^n=\frac{(\varepsilon\rho_g)_i^n+(\varepsilon\rho_g)_{i+1}^n}{2} \qquad (43)$$

Equation (36) eliminates the particle velocity, v_p^{n+1}, in equation (42) and gives an exchange term that is independent of the unknown velocity. The resulting expression contains only gas phase parameters and other terms that can be computed explicitly:

$$E_x=C_{i+\frac{1}{2}}\frac{P_{i+1}^{n+1}-P_i^{n+1}}{\Delta x}-A_{i+\frac{1}{2}}(\varepsilon\rho_g u_g)_{i+\frac{1}{2}}^{n+1}+B_{i+\frac{1}{2}}-D_{i+\frac{1}{2}}\frac{\tau_{i+1}^{n+1}-\tau_i^{n+1}}{\Delta x} \qquad (44)$$

The explicit coefficients, A, B, C and D are given in Appendix A. It is worth noting that the C coefficient is an approximation for θ and so the pressure gradient terms of equations (41) and (44) reduce to an appropriate representation of the term in equation (2).

An explicit formulation for the gas momentum convective term was chosen to keep the system of equations linear, this term is calculated using an upwind procedure as:

$$(\varepsilon\rho_g u_g^2)_i^n=\frac{m_{i+\frac{1}{2}}^n+m_{i-\frac{1}{2}}^n}{2}\cdot\begin{cases}(u_g)_{i-\frac{1}{2}}^n & \text{if } m_{i+\frac{1}{2}}^n+m_{i-\frac{1}{2}}^n>0\\(u_g)_{i+\frac{1}{2}}^n & \text{if } m_{i+\frac{1}{2}}^n+m_{i-\frac{1}{2}}^n<0\end{cases} \qquad (45)$$

where $m_{i+\frac{1}{2}}^n=(\varepsilon\rho_g u_g)_{i+\frac{1}{2}}^n$ so $m_{i+\frac{1}{2}}^n+m_{i-\frac{1}{2}}^n$ is an evaluation of the mass flux at the point i.

The solid phase momentum flux, equation (39), can be written as:

$$(\rho_s\theta\delta u_s)_{i+\frac{1}{2}}=\rho_s\Delta tA_{i+\frac{1}{2}}(\rho_g\varepsilon u_g)_{i+\frac{1}{2}}^{n+1}-\rho_s\Delta tF_{i+\frac{1}{2}}-C_{i+\frac{1}{2}}\frac{P_{i+1}^{n+1}-P_i^{n+1}}{\Delta x}-E_{i+\frac{1}{2}}\frac{\tau_{i+1}^{n+1}-\tau_i^{n+1}}{\Delta x} \qquad (46)$$

Appendix A gives the coefficients. The terms P_i^{n+1} and τ_i^{n+1} are linearized in terms of θ and $\varepsilon\rho_g$ as:

$$P_i^{n+1}=P_i^n+\left(\frac{\partial P}{\partial\rho}\right)_i^n(\Delta\rho) \qquad (47)$$

but $\rho_{gi}^n=\frac{(\varepsilon\rho_g)_i^n}{1-\theta_i^n}$ so $\Delta\rho=\frac{(\varepsilon\rho_g)_i^{n+1}-(\varepsilon\rho_g)_i^n}{1-\theta_i^n}+\frac{(\varepsilon\rho_g)_i^n}{(1-\theta_i^n)^2}\left(\theta_i^{n+1}-\theta_i^n\right)$.

Similarly $$\tau_i^{n+1} = \tau_i^n + \left(\frac{\partial \tau}{\partial \theta}\right)_i^n \left(\theta_i^{n+1} - \theta_i^n\right) \quad (48)$$

Summary of numerical formulation

We now have all the necessary evaluations. The final four Eulerian equations are summarized as:

$$\frac{(\theta\rho_s)_i^{n+1} - (\theta\rho_s)_i^n}{\Delta t} + \left.\frac{\partial(\theta\rho_s u_s)}{\partial x}\right|_{explicit} + \frac{(\theta\rho_s \delta u_s)_{i+\frac{1}{2}} - (\theta\rho_s \delta u_s)_{i-\frac{1}{2}}}{\Delta x} = 0 \quad (49)$$

$$\frac{(\varepsilon\rho_g)_i^{n+1} - (\varepsilon\rho_g)_i^n}{\Delta t} + \frac{(\varepsilon\rho_g u_g)_{i+\frac{1}{2}}^{n+1} - (\varepsilon\rho_g u_g)_{i-\frac{1}{2}}^{n+1}}{\Delta x} = 0 \quad (50)$$

$$(\theta\rho_s \delta u_s)_{i+\frac{1}{2}} = \Delta t A_{i+\frac{1}{2}} (\varepsilon\rho_g u_g)_{i+\frac{1}{2}}^{n+1} - \Delta t \rho_s F_{i+\frac{1}{2}} - C_{i+\frac{1}{2}} \frac{P_{i+1}^{n+1} - P_i^{n+1}}{\Delta x} - E_{i+\frac{1}{2}} \frac{\tau_{i+1}^{n+1} - \tau_i^{n+1}}{\Delta x} \quad (51)$$

$$\frac{(\varepsilon\rho_g u_g)_{i+\frac{1}{2}}^{n+1} - (\varepsilon\rho_g u_g)_{i+\frac{1}{2}}^n}{\Delta t} + \frac{(\varepsilon\rho_g u_g^2)_{i+1}^n - (\varepsilon\rho_g u_g^2)_i^n}{\Delta x} + \frac{P_{i+1}^{n+1} - P_i^{n+1}}{\Delta x} = C_{i+\frac{1}{2}} \frac{P_{i+1}^{n+1} - P_i^{n+1}}{\Delta x} - A_{i+\frac{1}{2}} (\varepsilon\rho_g u_g)_{i+\frac{1}{2}}^{n+1} + B_{i+\frac{1}{2}} - D_{i+\frac{1}{2}} \frac{\tau_{i+1}^{n+1} - \tau_i^{n+1}}{\Delta x} - (\varepsilon\rho_g)_{i+\frac{1}{2}}^n g \quad (52)$$

where the solid continuity equation is written in terms of $\theta\rho_s$ for consistency with the gas phase continuity equations. The fluxes $\theta\rho_s \delta u_s$ and $\varepsilon\rho_g u_g$, and the pressure and stress terms use the linearized forms of equations (47) and (48).

Solution procedure

Equations (49) to (52) are a set of linear equations relating the variables $\theta\rho_s$, $\varepsilon\rho_g$, $\theta\rho_s \delta u_s$, and $\varepsilon\rho_g u_g$. The parameters A, B, C, D, E, and F are explicitly calculated. Equations (51) and (52) are rewritten as linear functions of $\theta\rho_s$ and $\varepsilon\rho_g$ and substituted into equations (49) and (50). The results are two equations per node relating $(\theta\rho_s)_i^{n+1}$ and $(\varepsilon\rho_g)_i^{n+1}$ to their neighbors and themselves. A Conjugate Residual method has been used to solve this linear equation set. The n+1 values for $\theta\rho_s$ and $\varepsilon\rho_g$ are then substituted into equation (52) to give $\varepsilon\rho_g u_g$ and u_g. Equation (37) is then used to update the particle velocities.

The cell-particle coefficients A to F are well suited to a massively parallel computation where each particle is assigned an individual processor.

TEST PROBLEMS

Three test problems are described and solved. Each problem uses a low particle Reynolds number so that in the first two problems the computed solutions can be compared with analytical ones. The third problem uses two particle sizes in a slug deposition problem that demonstrates the power of the new method. Prior to these three test problems we performed two simple checks. The first check used no particles and zero gravity, and the second check used zero gravity and initially stationary particles. The first check ensured no spurious sources were introduced. The second check was to see if the position of the particles changed over time. If they did, it implied that the interpolation procedure was incorrectly spreading errors. Both checks were successful and led to the following more elaborate tests.

Single particle under free free-fall

In this problem we compute the free-fall of a single particle starting from rest. Table 1 describes the test conditions and physical parameters. The test parameters are in SI units with values chosen for convenient non-dimensionalization, and to give a low particle Reynolds number of 0.01. At this low Reynolds number the drag term reduces to Stokes drag and equation (20) may be solved to give the particle velocity:

$$v_p = \frac{g}{D}\left(\frac{\rho_g - \rho_s}{\rho_s}\right)\left(1 - e^{-Dt}\right) \quad \text{with} \quad D = \frac{9}{2}\frac{\mu_g}{\rho_s r^2} \quad (53)$$

Substituting the values of Table 1 gives a free fall velocity, v_∞ = 0.1 and a Stokes time scale 1/D of 1/90. Figure 4 shows the computed and analytical results for the development of the free fall velocity. The particle velocity has been normalized by the analytical free-fall velocity, v_∞, and time by the Stokes time scale 1/D. The agreement is excellent and the normalized computed free fall and analytical velocity at the end were 0.986571 and 0.993261 respectively. The 0.67% error can be attributed to assumptions in obtaining the analytical result that are not made for the computed one.

Gas density	1.0 kg/m^3
Gas viscosity	2.0 x 10^{-2} kg/(m s)
Solid density	10^3 kg/m^3
Gravity (g)	9 m/s^2
Particle mass	4.18879 x 10^{-6} kg
Particle radius	10^{-3} m
Length of domain (x_{last})	1.0 m
Number of cells (N_{cell})	10
Simulated time (t_{last})	5.555 x 10^{-2}s , i.e. 5/D
Time step (Δt)	t_{last}/100

Table 1. Parameters for the single particle computation.

A slug of particles under free fall

This problem extends the single particle problem to a slug of particles that settle under free fall. Table 2 shows the parameters for the computation. The slug of particles is defined by placing 250 equally spaced parcels, each with 100 particles, between x = 0.6 and 0.8 m. A total of 25 uniformly spaced cells spanned the computational domain of 1 m. Thus, cells from 16 to 20 contain 50 parcels each for a total of 5000 particles per cell. The resulting initial solid void fraction, θ_0, is 5.223575 x 10^{-4}. This low solids void

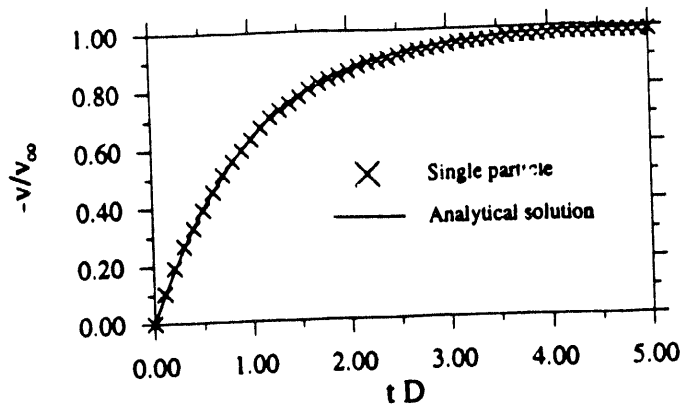

Figure 4. Velocity rise of a single particle under free-fall.

fraction was chosen so that the void fraction dependence of the drag coefficient in equation (16) could be neglected. Adding of the mass continuity equations for solid and gas phases and noting that net mass flux below the slug is zero gives:

$$\theta v_p + \varepsilon u_g = 0 \qquad (54)$$

Neglecting inertial terms and noting that spatial gradients are negligible results in the following two simultaneous equations:

$$\varepsilon\frac{\partial u_g}{\partial t} + \frac{\varepsilon}{\rho_g}\frac{\partial P}{\partial x} = -\varepsilon g - D\theta\frac{\rho_s}{\rho_g}(u_g - v_p)$$
$$\theta\frac{\partial v_p}{\partial t} + \frac{\theta}{\rho_s}\frac{\partial P}{\partial x} = -\theta g - D\theta(u_g - v_p) \qquad (55)$$

Using equation (63) and eliminating the pressure gradient gives the following results for particle and gas velocity:

$$v_p = \frac{\varepsilon^2 g}{D}\left(\frac{\rho_g - \rho_s}{\rho_s}\right)\left(1 - e^{-\frac{D\rho_s}{d(\varepsilon\rho_s + \theta\rho_s)}t}\right) \text{ and } u_g = -\frac{\theta}{\varepsilon}v_p \qquad (56)$$

For a single particle $\theta \cong 0$ and this result reduces to equation (53).

Figure 5 shows the slug of particles as a solids void fraction normalized by θ_0 at a sequence of times starting with the initial condition at the top. Figure 2 shows that the edges of the void

Gas density	1.0 kg/m^3
Gas viscosity	2.0 x 10^{-2} kg/(m s)
Solid density	10^3 kg/m^3
Gravity (g)	9 m/s^2
Particle mass	4.18879 x 10^{-6} kg
Particle radius	10^{-3} m
No. of particles per parcel	100
Length of domain (x_{last})	1.0 m
Number of cells (N_{cell})	25
Simulated time (t_{last})	4 s
Time step (Δt)	1 x 10^{-3} s

Table 2. Parameters for the falling slug computation.

fraction are rounded because of the linear interpolation function. The figure shows that the slug falls at constant velocity. The free-fall velocity from equation (65) is -0.099895, which is slightly below the single particle velocity of -0.1 because of the ε^2 dependence. The

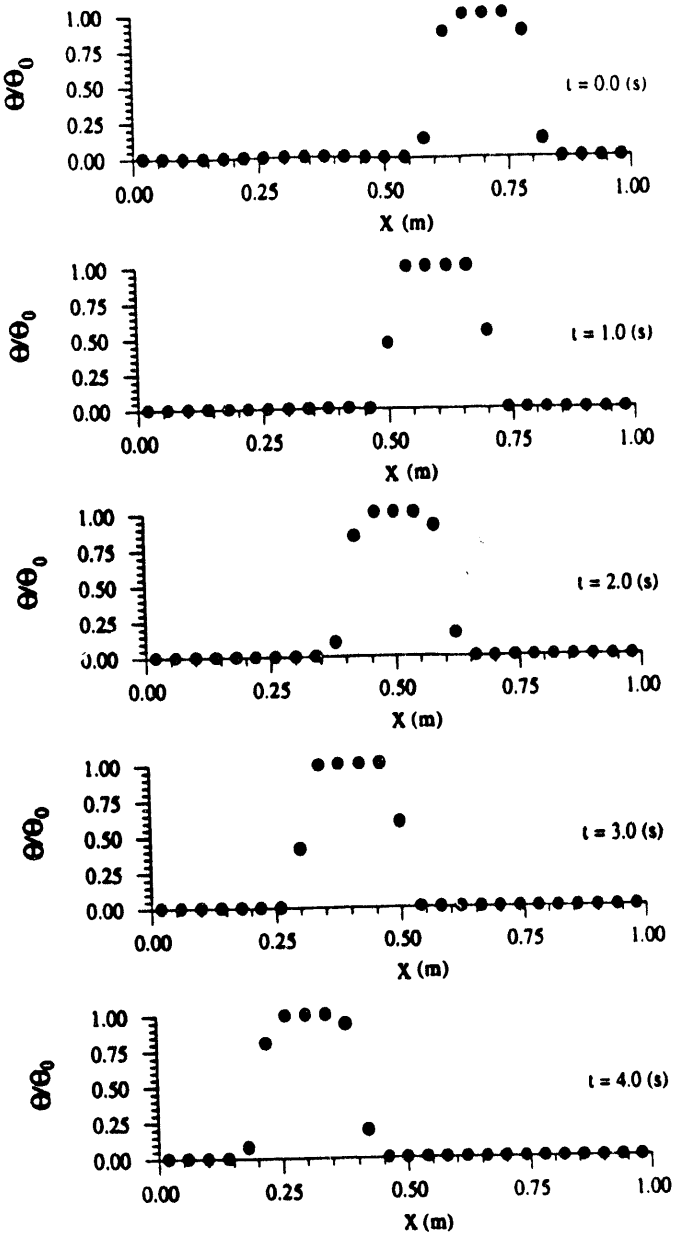

Figure 5. Computed solid void fraction of a falling slug of particles.

computed particle free fall velocity was -0.09909 and in reasonable agreement with the analytical result. Similarly, the computed gas velocity was 5.242421 x 10^{-5} and in reasonable agreement with the expected value from equation (56) of 5.218 x 10^{-5}.

The computational cell size is 0.04 and the slug velocity is close to 0.1, so the slug traverses 5 computational cells every 2 s. Therefore, the void fraction plots at 0, 2 and 4 s, and at 1 and 3 s should be comparable. Inspection of figure 5 reveals that, besides the displacement, the values at time 2 and 4 seconds, and 1 and 3 s are practically identical. A small difference can be seen between 1 and 2 s and may be attributed to the finite time rise of the slug velocity to its free fall value. Parenthetically, this retention of solids void fraction profile demonstrates that because of its particle nature our multi-phase calculation procedure has low numerical diffusion.

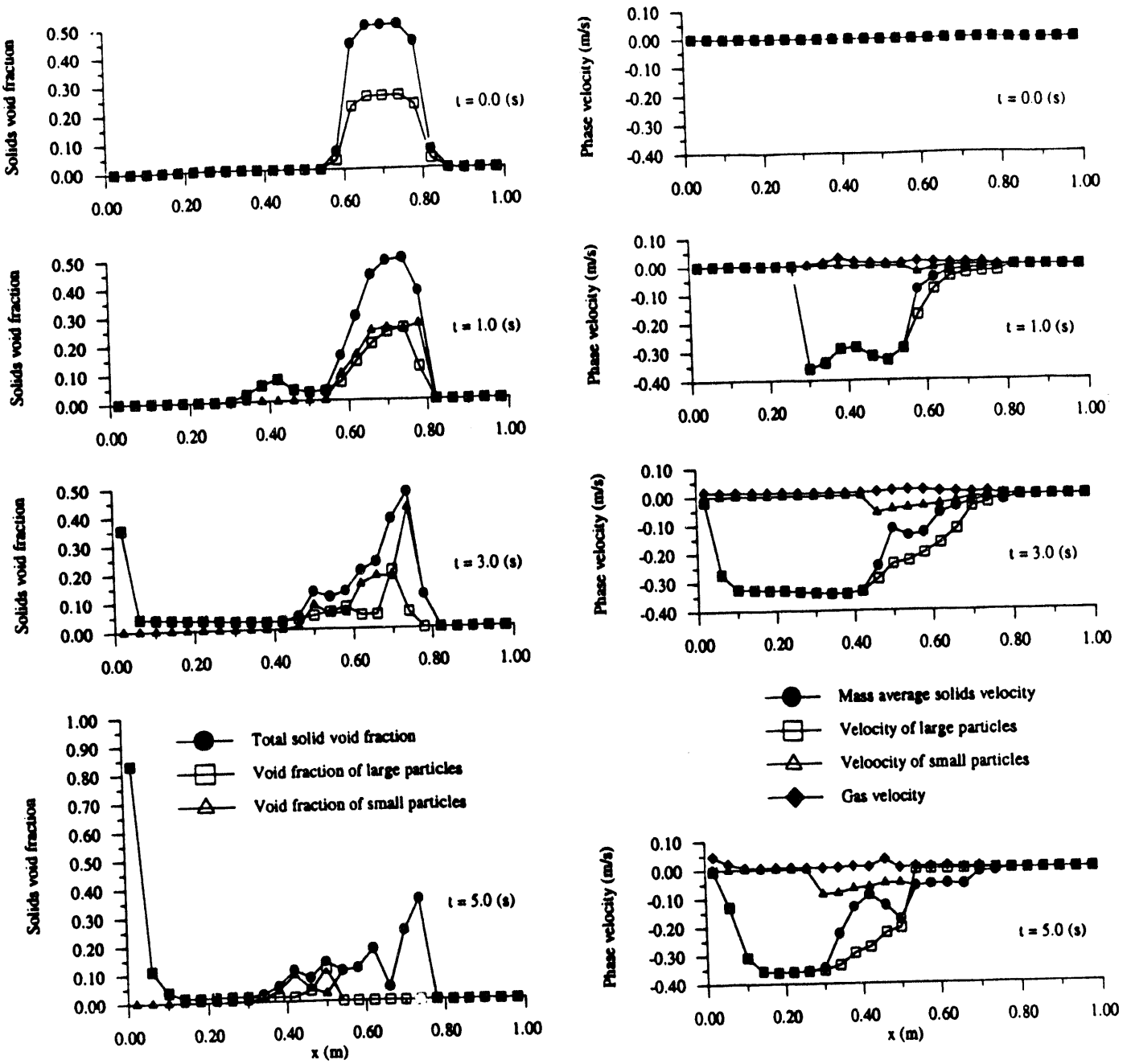

Figure 6. Solid void fractions and phase velocities for the bi-modal slug sedimentation test problem.

Sedimentation of a packed slug of two particle sizes

The last problem combines elements of the first two but uses equal volume fractions of two particle sizes: one with a particle radius of 1 mm and the other 2 mm. The solid particles form a slug of material evenly distributed between x = 0.6 m and 0.8 m. A total of 530 parcels for each particle size per cell was used with 22,500 small particles per parcel and 2,813 large particles per parcel. These particle and parcel specifications gave an initial void fraction of each particle size of 0.25 and a dense region of solid particles with net void fraction of 0.5. Table 3 presents additional details of the computational. Figure 6 shows the initial solids void fraction, with the particles and gas initially stationary. The remaining test parameters are those of the previous two test problems and so similar development time scales are expected.

Figure 6 shows the computed sedimentation of the slug. The left side of the figure shows the development of solids void fraction (void fraction of the small particles, large particles, and total), and the right side of the figure shows the phase velocities (gas velocity, velocity of small particles, large particles, and mass average solids velocity). Inspection of the solids void fraction profiles reveals, as expected, that the small particles sediment more slowly to the bottom than the large particles because of their higher surface to volume ratio. The

Gas density	1.0 kg/m^3
Gas viscosity	2.0 x 10^{-2} kg/(m s)
Solid density	10^3 kg/m^3
Gravity (g)	9 m/s^2
Small particle mass	4.18879 x 10^{-6} kg
Small particle radius	10^{-3} m
No. of small particles per parcel	22,500
Large particle mass	3.35103 x 10^{-5} kg
Large particle radius	2 x 10^{-3} m
No. of large particles per parcel	2,813
Length of domain (x_{last})	1.0 m
Number of cells (N_{cell})	25
Simulated time (t_{last})	5 s
Time step (Δt)	1 x 10^{-3} s

Table 3. Parameters for the slug sedimentation problem.

figure shows that a slope develops in the volume fraction on the bottom of the slug as the slug sediments through the gas. Test problem 2 did not develop such a slope and the slug boundaries remained steep and well defined. The key difference in the two cases is the much larger void fraction in test problem 3. Equation (54) applies for test problem 2 and since there is only a small solids void fraction and, consequently, only a small variation, the gas velocity is approximately constant with a small value compared with the particle velocity. However, the solid void fraction in test problem 3 has a much greater value and variation, so the gas velocity from equation (54) is high in the regions of high solids void fraction and low in regions of low solids void fraction. This effect is noticeable at t = 5 s at the bottom of the domain where the gas velocity is much higher than the solids velocity. The variation of gas velocity along the void fraction profile effects the particle velocities because of drag, and gives a higher particle velocity when the gas velocity is small (low solids void fraction) and lower particle velocities when the gas velocity is large (high solids void fraction).

The right-hand side of figure 6 shows an increase of particle velocity with a decrease in solids void fraction. It is evident from the figure that large particles fall faster than small ones and that as the solids fall the gas rises to fill the volume. The average mass velocity is biased toward the larger particles because each has 8 times the mass of a small particle. This bias creates the peaks and dips in the mass average velocity profile. Oscillations along the void fraction profiles may be numerical or physical.

The total solids void fraction at the top of the slug (about 0.8 m) at a time of 5 s contains no large particles and consequently is the void fraction of the small particles. The small particle void fraction value of 0.4 would appear anomalous, since this is larger than the initial void fraction of 0.25. This sharpening of the slug boundary by small particles can be attributed to the dependence of the particle drag on gas void fraction, equation (16). A higher gas void fraction results in a low drag coefficient so a particle left behind the slug in a region of higher gas void fraction falls faster and rejoins the slug. Thus, a sharp interface forms at the top of the slug.

CONCLUSIONS

A new methodology for simulation of multi-phase granular flows has been presented. The method uses a combined Lagrangian/Eulerian formulation that computes the development of the particle distribution function with a Lagrangian technique and accounts for continuum intergranular stress with an Eulerian formulation. An accurate mapping to and from the Lagrangian and Eulerian grid allows the most accurate physical and numerical formulation to be chosen. The formulation of particle-cell coefficients is well suited to massively parallel computation.

The methodology has been developed into a computer code for one-dimensional problems and demonstrated on three test problems. The first two test problems successfully compared with analytical solutions. The second problem showed that our method also suffers from low numerical diffusion. The third test problem showed the sedimentation of a slug of densely packed solid particles of two sizes. Calculated sedimentation profiles showed complex particle-gas interactions and the formation of a well-defined interface on the high side of the slug due to a decrease in drag coefficient. As expected, the larger particles fell faster and separated from the small particles.

The three test problems show that this Lagrangian/Eulerian method works well and is suited to the simulation of multi-phase flow problems with a wide range of particulate characteristics. The next step is to extend the one-dimensional formulation to two-dimensions and to investigate the use of a more fundamental approach for the computation of solids stress.

ACKNOWLEDGMENTS

An Engineering Excellence Grant from Texas A&M University supported Andrews. Support for Baillergeau's work was provided by Ecole Polytechnique while he was a research intern at Los Alamos National Laboratory during the summer of 1993. O'Rourke's work was supported by the U.S. Department of Energy, Office of Conservation and Renewable Energy, Advanced Industrial Concepts Division.

REFERENCES

Andrews, M.J., 1993, "The Large-Scale Fragmentation of the Intact Liquid Core of a Spray Jet," *Atomization and Sprays*, Vol. 3, No. 1.

Andrews, M.J. and Bracco, F.V., 1988, "On The Structure of Turbulent Dense Spray Jets," in *Volume 8 of the Encyclopedia of Fluid Mechanics*, Ed N.P. Chereminisoff.

Gidaspow, D., 1986, "Hydrodynamics of Fluidization and Heat Transfer: Supercomputer Modeling," *Appl. Mech. Rev.* Vol. 39, No. 1.

Harlow, F.H., 1964, "The Particle-in-Cell Computing Method of Fluid Dynamics," *Fundamental Methods in Hydrodynamics*, edited by B. Alder, S. Fernbach and M. Rotenberg, Academic Press, NY.

Kuo, K.K., 1986, "Principles of Combustion," *John Wiley and Sons*.

O'Rourke, P.J., 1981, "Collective Drop Effects on Vaporizing Liquid Sprays," Ph.D. Thesis, *Princeton University*.

Putnam, A., 1961, ARS J. Vol. 31, p. 1367.

Richardson, J. F., and Zaki, W. N., 1954, "Sedimentation and Fluidization: Part I," Trans. I. *Chem. Engrs.*, 32, pp. 35-53.

Rizk, M.A.,1993, "Mathematical Modeling of Densely Loaded, Particle-Laden, Turbulent Flows," *Atomization and Sprays*, Vol. 3, No. 1.

APPENDIX A: EVALUATION OF NUMERICAL COEFFICIENTS

$$A_{i+\frac{1}{2}} = \frac{1}{\Delta x (\rho_g \varepsilon)^n_{i+\frac{1}{2}}} \sum_p \left[N_p m_p T_{i+\frac{1}{2}}(\tilde{x}_p) \frac{D^n_p}{1 + \Delta t D^n_p} \right] \tag{57}$$

$$B_{i+\frac{1}{2}} = \frac{1}{\Delta x} \sum_p \left[N_p m_p T_{i+\frac{1}{2}}(\tilde{x}_p) \frac{D^n_p (v^n_p - \Delta t g)}{1 + \Delta t D^n_p} \right] \tag{58}$$

$$C_{i+\frac{1}{2}} = \frac{1}{\Delta x} \sum_p \left[N_p \frac{m_p}{\rho_i} T_{i+\frac{1}{2}}(\tilde{x}_p) \frac{1}{1 + \Delta t D^n_p} \right] \tag{59}$$

$$D_{i+\frac{1}{2}} = \frac{1}{\Delta x \tilde{\theta}_{i+\frac{1}{2}}} \sum_p \left[N_p \frac{m_p}{\rho_i} T_{i+\frac{1}{2}}(\tilde{x}_p) \frac{\Delta t D^n_p}{1 + \Delta t D^n_p} \right] \tag{60}$$

$$E_{i+\frac{1}{2}} = \frac{1}{\tilde{\theta}_{i+\frac{1}{2}} \Delta x} \sum_p \left[N_p \frac{m_p}{\rho_i} T_{i+\frac{1}{2}}(\tilde{x}_p) \frac{1}{1 + \Delta t D^n_p} \right] \tag{61}$$

$$F_{i+\frac{1}{2}} = \frac{1}{\Delta x} \sum_p \left[N_p \frac{m_p}{\rho_i} T_{i+\frac{1}{2}}(\tilde{x}_p) \frac{D^n_p v^n_p + g}{1 + \Delta t D^n_p} \right] \tag{62}$$

DATE
FILMED
10/19/94

END